PLOS ONE

RESEARCH ARTICLE

MHD Convective Flow of Jeffrey Fluid Due to a Curved Stretching Surface with Homogeneous-Heterogeneous Reactions

Maria Imtiaz[1]*, Tasawar Hayat[1,2], Ahmed Alsaedi[2]

1 Department of Mathematics, Quaid-I-Azam University, 45320, Islamabad, 44000, Pakistan, **2** Nonlinear Analysis and Applied Mathematics (NAAM) Research Group, Department of Mathematics, Faculty of Science, King Abdulaziz University, 80203, Jeddah, 21589, Saudi Arabia

* mi_qau@gmail.com

Abstract

This paper looks at the flow of Jeffrey fluid due to a curved stretching sheet. Effect of homogeneous-heterogeneous reactions is considered. An electrically conducting fluid in the presence of applied magnetic field is considered. Convective boundary conditions model the heat transfer analysis. Transformation method reduces the governing nonlinear partial differential equations into the ordinary differential equations. Convergence of the obtained series solutions is explicitly discussed. Characteristics of sundry parameters on the velocity, temperature and concentration profiles are analyzed by plotting graphs. Computations for pressure, skin friction coefficient and surface heat transfer rate are presented and examined. It is noted that fluid velocity and temperature through curvature parameter are enhanced. Increasing values of Biot number correspond to the enhancement in temperature and Nusselt number.

Citation: Imtiaz M, Hayat T, Alsaedi A (2016) MHD Convective Flow of Jeffrey Fluid Due to a Curved Stretching Surface with Homogeneous-Heterogeneous Reactions. PLoS ONE 11(9): e0161641. doi:10.1371/journal.pone.0161641

Editor: Zhong-Ke Gao, Tianjin University, CHINA

Received: April 26, 2016

Accepted: August 9, 2016

Published: September 1, 2016

Data Availability Statement: All relevant data is within the paper.

Funding: The author(s) received no specific funding for this work.

Competing Interests: The authors have declared that no competing interests exist.

1. Introduction

The study of non-Newtonian fluids has gained special focus of the recent researchers and engineers. Such motivation of the researchers is due to various applications of non-Newtonian fluids in technology and industrial areas. Unlike the viscous materials, the non-Newtonian fluids cannot be explained using well known Navier-Stokes theory. A single constitutive relationship cannot describe the characteristics of non-Newtonian liquids. The facts of non-Newtonian fluids are distinct than the viscous materials. The order of differential system in non-Newtonian fluid situation is higher than the viscous material. There are many proposed models of non-Newtonian fluids with diverse properties. These fluids in general have been classified into three categories known as the rate, the differential and the integral types. The most common and simplest model of non-Newtonian fluids is Jeffrey fluid. Such fluid has time derivative instead of convected derivative. Aspects of retardation and relaxation times are described by this fluid model. MHD flow of Jeffrey fluid in a cylindrical tube has been studied by Tripathi et al. [1]. Influences of slip and heat transfer on MHD peristaltic flow of Jeffrey fluid have been examined by Das [2]. Variable thermal conductivity of Jeffrey fluid in presence of thermal jump has been analyzed by Hamad et al. [3]. Shehzad et al. [4] presented the nonlinear thermal radiation effect in three dimensional flow

of Jeffrey nanofluid. Ellahi and Hussain [5] examined slip feature in flow of Jeffrey fluid. Hayat et al. [6] studied stagnation point flow of Jeffrey nanofluid in presence of Newtonian heating. Flow of Jeffrey fluid due to oscillation of disks has been studied by Reddy et al. [7]. Farooq et al. [8] analyzed MHD flow of Jeffrey fluid in presence of Newtonian heating.

Many chemically reacting systems involve homogeneous-heterogeneous reactions for example in biochemical systems, combustion and catalysis. The correlation between homogeneous and heterogeneous reactions is very complex. Some of the reactions have the ability to proceed very slowly or not at all except in the presence of a catalyst. Fog formation and dispersion, food processing, ceramics and polymer production, hydrometallurgical industry etc. show obvious involvement of chemical reaction. Merkin [9] studied homogeneous-heterogeneous reactions in flow of viscous fluid over a flat plate. He considered homogeneous reaction for cubic autocatalysis and heterogeneous reaction on the catalyst surface. It is shown that surface reaction dominants near the plate. Homogenous-heterogeneous reactions with equal diffusivities have been examined by Chaudhary and Merkin [10]. Homogeneous-heterogeneous reactions in stretched flow of viscous fluid have been investigated by Bachok et al. [11]. Khan and Pop [12] presented stretched flow of viscoelastic fluid in presence of homogeneous-heterogeneous reactions. Shaw et al. [13] studied homogeneous-heterogeneous reactions in flow of micropolar fluid. Homogeneous-heterogeneous reactions in nanofluid flow over a permeable stretching surface have been analyzed by Kameswaran et al. [14]. Hayat et al. [15] investigated three dimensional flow of nanofluid in presence of second order slip velocity and homogeneous—heterogeneous reactions. Hayat et al. [16] also examined Cattaneo-Christov heat flux in MHD flow of Oldroyd-B fluid. Here homogeneous-heterogeneous reactions are considered.

Two-phase flow has wide applications in many industrial processes such as natural gas networks, spray processes, lubrication and nuclear reactor cooling. Main difference between single phase flow and multiphase flow is the existence of flow pattern which indicates a flow situation uniquely defined by the temporal and spatial distribution of the two immiscible phases. Three typical gas-liquid flow patterns are bubble flow, slug flow and churn flow. Research interests in the characterization of flow patterns lie on the fact that different flow patterns have distinct nonlinear dynamical properties. The recent advances in the study of multiphase flow are presented by Gao et al. [17–20].

Fluid flow by a stretching surface has promising applications in engineering and industrial processes such as in paper production, manufacture of foods, glass fiber, drawing of wires and plastic films, liquid films in condensation process, crystal growing, manufacturing and extraction of polymer and rubber sheets etc. Flow caused by stretching of a sheet has been examined by Crane [21]. After that stretched flow problems under different configurations have been examined by several researchers. Cortell [22] studied radiative nonlinear heat transfer in flow over a stretching sheet. Hsiao [23, 24] presented mixed convection effect in MHD flow of viscoelastic fluid past a stretching sheet with ohmic dissipation. Hsiao [25] examined MHD mixed convection for viscoelastic fluid past a porous wedge. Slip effect in stretched flow of nanofluid have been studied by Malvandi et al. [26]. Hsiao [27] investigated MHD stagnation point flow of nanofluid over a stretching sheet with mixed convection and partial slip. Sheikholeslami et al. [28] discussed effect of thermal radiation in magnetohydrodynamic nanofluid flow over a stretching sheet. Lin et al. [29] analyzed flow of pseudo-plastic nanoliquid over a stretching surface. In all these articles flat sheet is stretched and Cartesian coordinate system is used for mathematical modeling. Sajid et al. [30] provided fluid flow due to curved stretching sheet. They used curvilinear coordinate system in order to obtain the governing equations. They found that pressure is not negligible inside the boundary layer as in the case of a flat stretching sheet. Naveed et al. [31] studied MHD flow by a curved stretching surface. Time-dependent fluid flow due to curved stretching/shrinking surface has been presented by Rosca and Pop

[32]. Radiative flow of nanofluid by a curved stretching surface with partial slip has been examined by Abbas et al. [33].

Main objective of present study is to extend the flow analysis of Sajid et al. [30] into following directions. Firstly, to model flow analysis for Jeffrey fluid. Secondly to predict the influence of homogeneous-heterogeneous reactions. Thirdly to examine heat transfer analysis in the presence of convective boundary conditions. Series solutions of present problem are computed by homotopy analysis method (HAM) [34–42]. The behaviors of different parameters on the physical quantities have been examined. Pressure, surface drag force and heat transfer rate are also studied. We hope that this study will lead to further investigations in future for various flow geometries and different flow models.

2. Model development

Consider two-dimensional flow of Jeffrey fluid induced by a curved stretching sheet at $r = R$. Stretching of sheet is taken in the x – direction with velocity $u = u_w$. A magnetic field of strength B_0 is applied in the r – direction. Also the bottom surface of sheet is heated by convection from a hot fluid at temperature T_f while ambient fluid temperature is T_∞. Homogeneous-heterogeneous reactions of two chemical species A and B are considered. For cubic autocatalysis, the homogeneous reaction is

$$A + 2B \rightarrow 3B, \qquad \text{rate} = k_c ab^2, \tag{1}$$

while heterogeneous reaction on the catalyst surface is

$$A \rightarrow B, \qquad \text{rate} = k_s a, \tag{2}$$

where rate constants are defined by k_c and k_s and the chemical species A and B have concentrations a and b. Governing equations of present boundary layer flow problem are

$$(r+R)\frac{\partial v}{\partial r} + v + R\frac{\partial u}{\partial x} = 0, \tag{3}$$

$$\frac{u^2}{r+R} = -\frac{1}{\rho}\frac{\partial p}{\partial r}, \tag{4}$$

$$\begin{aligned} v\frac{\partial u}{\partial r} + \frac{Ru}{r+R}\frac{\partial u}{\partial x} + \frac{uv}{r+R} = -\frac{1}{\rho}\frac{R}{r+R}\frac{\partial p}{\partial x} + \frac{\nu}{1+\lambda_1}\Bigg[\frac{\partial^2 u}{\partial r^2} + \frac{1}{r+R}\frac{\partial u}{\partial r} \\ - \frac{u}{(r+R)^2} + \lambda_2\Bigg(\frac{\partial v}{\partial r}\frac{\partial^2 u}{\partial r^2} + v\frac{\partial^3 u}{\partial r^3} + \frac{R}{r+R}\frac{\partial u}{\partial r}\frac{\partial^2 u}{\partial x \partial r} + \frac{R}{r+R}u\frac{\partial^3 u}{\partial x \partial r^2} \\ + \frac{1}{r+R}v\frac{\partial^2 u}{\partial r^2} - \frac{R}{(r+R)^2}\frac{\partial u}{\partial r}\frac{\partial u}{\partial x} - \frac{1}{r+R}\frac{\partial v}{\partial r}\frac{\partial u}{\partial r} \\ + \frac{1}{(r+R)^2}u\frac{\partial v}{\partial r}\Bigg)\Bigg] - \frac{\sigma B_0^2 u}{\rho}, \end{aligned} \tag{5}$$

$$v\frac{\partial T}{\partial r}+\frac{Ru}{r+R}\frac{\partial T}{\partial x}=\alpha^{*}\left(\frac{\partial^{2}T}{\partial r^{2}}+\frac{1}{r+R}\frac{\partial T}{\partial r}\right), \tag{6}$$

$$v\frac{\partial a}{\partial r}+\frac{Ru}{r+R}\frac{\partial a}{\partial x}=D_{A}\left(\frac{\partial^{2}a}{\partial r^{2}}+\frac{1}{r+R}\frac{\partial a}{\partial r}\right)-k_{c}ab^{2}, \tag{7}$$

$$v\frac{\partial b}{\partial r}+\frac{Ru}{r+R}\frac{\partial b}{\partial x}=D_{B}\left(\frac{\partial^{2}b}{\partial r^{2}}+\frac{1}{r+R}\frac{\partial b}{\partial r}\right)+k_{c}ab^{2}, \tag{8}$$

with boundary conditions

$$\begin{aligned} &u=u_{w}=cx,\ v=0,\ k_{f}\frac{\partial T}{\partial r}=h(T_{f}-T),\ D_{A}\frac{\partial a}{\partial r}=k_{s}a,\ D_{B}\frac{\partial b}{\partial r}=-k_{s}a \text{ at } r=0,\\ &u\to 0,\ \frac{\partial u}{\partial r}\to 0,\ T\to T_{\infty},\ a\to a_{0},\ b\to 0 \text{ as } r\to\infty, \end{aligned} \tag{9}$$

where the velocity components in (r,x) direction are (v,u) respectively, p denotes the pressure, ρ the density, σ the electrical conductivity, ν the kinematic viscosity, $c>0$ the stretching constant, λ_1 the ratio of relaxation to retardation times, λ_2 the retardation time, h the convective heat transfer coefficient, T the temperature, k_f the thermal conductivity and α^{*} the thermal diffusivity.

Using the following transformations

$$\begin{aligned} &u=cxf'(\xi),\ v=-\frac{R}{r+R}\sqrt{cv}f(\xi),\ \xi=\sqrt{\frac{c}{v}}r,\ p=\rho c^{2}x^{2}P(\xi),\\ &\theta(\xi)=\frac{T-T_{\infty}}{T_{f}-T_{\infty}},\ a=a_{0}\Phi(\xi),\ b=a_{0}g(\xi). \end{aligned} \tag{10}$$

Eq (3) is satisfied automatically and Eqs 4–8 can be reduced as follows:

$$\frac{\partial P}{\partial\xi}=\frac{f'^{2}}{\xi+K} \tag{11}$$

$$\begin{aligned} \frac{2K}{\xi+K}P=&\frac{K}{\xi+K}ff''+\frac{K}{(\xi+K)^{2}}ff'-\frac{K}{\xi+K}f'^{2}+\frac{1}{1+\lambda_{1}}\\ &\left[f'''+\frac{1}{\xi+K}f''-\frac{1}{(\xi+K)^{2}}f'+\lambda\left\{\frac{K}{\xi+K}f''^{2}-\frac{K}{\xi+K}ff^{iv}-\frac{K}{(\xi+K)^{3}}ff''\right.\right.\\ &\left.\left.+\frac{K}{(\xi+K)^{4}}ff'-\frac{K}{(\xi+K)^{3}}f'^{2}\right\}\right]-Mf', \end{aligned} \tag{12}$$

$$\frac{1}{\mathrm{Pr}}\left(\theta''+\frac{1}{\xi+K}\theta'\right)+\frac{K}{\xi+K}f\theta'=0, \tag{13}$$

$$\frac{1}{Sc}\left(\Phi'' + \frac{1}{\xi + K}\Phi'\right) + \frac{K}{\xi + K} f\Phi' - k_1 \Phi g^2 = 0, \tag{14}$$

$$\frac{\delta}{Sc}\left(g'' + \frac{1}{\xi + K} g'\right) + \frac{K}{\xi + K} fg' + k_1 \Phi g^2 = 0, \tag{15}$$

$$\begin{aligned} &f'(0) = 1,\ f(0) = 0,\ \theta'(0) = -\gamma_1[1 - \theta(0)],\ \Phi'(0) = k_2\Phi(0),\ \delta g'(0) = -k_2\Phi(0), \\ &f'(\infty) \to 0,\ f''(\infty) \to 0,\ \theta(\infty) \to 0,\ \Phi(\infty) \to 1,\ g(\infty) \to 0, \end{aligned} \tag{16}$$

where $M = \sigma B_0^2/\rho c$ is the Hartman number, $\lambda = \lambda_2 c$ is the Deborah number, $K = R\sqrt{c/\nu}$ is the curvature parameter, $\Pr = \nu / \alpha$ is the Prandtl number, $\delta = D_B / D_A$ is the ratio of diffusion coefficient, $Sc = \nu / D_A$ is the Schmidt number, $k_1 = a_0^2 k_c / c$ is the homogeneous reaction strength, $k_2 = k_s\sqrt{\nu}/D_A\sqrt{c}$ is the heterogeneous reaction strength and $\gamma_1 = h\sqrt{\nu}/k\sqrt{c}$ is the Biot number.

Now eliminating pressure P between Eqs 11 and 12, we obtain

$$\begin{aligned} &f^{iv} + \frac{2}{\xi + K} f''' + \frac{1}{(\xi + K)^3} f' - \frac{1}{(\xi + K)^2} f'' + \lambda\left(\frac{2K}{\xi + K} f'' f''' - \frac{K}{\xi + K} f' f^{iv} - \frac{K}{\xi + K} f f^{v}\right. \\ &\left. + \frac{3K}{(\xi + K)^4} f f'' - \frac{K}{(\xi + K)^3} f f''' - \frac{3K}{(\xi + K)^3} f' f'' - \frac{3K}{(\xi + K)^5} f f' + \frac{3K}{(\xi + K)^4} f'^2\right) \\ &+ (1 + \lambda_1)\left(\frac{K}{\xi + K}(f f''' - f' f'') + \frac{K}{(\xi + K)^2}(f f'' - f'^2) - \frac{K}{(\xi + K)^3} f f' - M f'' - \frac{M}{\xi + K} f'\right) \\ &= 0 \end{aligned} \tag{17}$$

with boundary conditions

$$f'(0) = 1,\ f(0) = 0,\ f'(\infty) \to 0,\ f''(\infty) \to 0. \tag{18}$$

Pressure can now be determined from Eq 12 as

$$\begin{aligned} P = &\frac{1}{2} f f'' + \frac{1}{2(\xi + K)} f f' - \frac{1}{2} f'^2 + \frac{1}{1 + \lambda_1}\left[\frac{\xi + K}{2K} f''' - + \frac{1}{2K} f'' - \frac{1}{2K(\xi + K)} f'\right. \\ &\left. + \lambda\left(\frac{1}{2} f'^2 - \frac{1}{2} f f^{iv} - \frac{1}{2(\xi + K)^2} f f'' \quad + \frac{1}{2(\xi + K)^3} f f' - \frac{1}{2(\xi + K)^2} f'^2\right)\right] - M\frac{\xi + K}{2K} f'. \end{aligned} \tag{19}$$

Here it is assumed that both chemical species have equal diffusion coefficients D_A and D_B, i.e. $\delta = 1$ and thus

$$\Phi(\xi) + g(\xi) = 1. \tag{20}$$

Now Eqs 14 and 15 yield

$$\frac{1}{Sc}\left(\Phi'' + \frac{1}{\xi + K}\Phi'\right) + \frac{K}{\xi + K} f\Phi' - k_1 \Phi(1 - \Phi)^2 = 0, \tag{21}$$

with the boundary conditions

$$\Phi'(0) = k_2\Phi(0),\ \Phi(\infty) \to 1. \tag{22}$$

Skin friction coefficient C_f and Nusselt number Nu are

$$C_f = \frac{\tau_{rx}}{\frac{1}{2}\rho u_w^2},\ Nu = \frac{xq_w}{k_f(T_w - T_\infty)}, \tag{23}$$

where τ_{rx} represents surface shear stress and q_w the wall heat flux which are given by

$$\tau_{rx} = \frac{\mu}{1+\lambda_1}\left[\frac{\partial u}{\partial r} - \frac{u}{r+R} + \lambda_2\left\{\frac{Ru}{r+R}\frac{\partial^2 u}{\partial x \partial r} - \frac{Ru}{(r+R)^2}\frac{\partial u}{\partial x}\right.\right.$$
$$\left.\left. + \nu\frac{\partial^2 u}{\partial r^2} - \frac{\nu}{r+R}\frac{\partial u}{\partial r} + \frac{uv}{(r+R)^2}\right\}\right]_{r=0}, \tag{24}$$

$$q_w = -k_f\left.\frac{\partial T}{\partial r}\right|_{r=0}. \tag{25}$$

Finally, we have

$$\frac{1}{2}C_f(\mathrm{Re}_x)^{1/2} = \frac{1}{1+\lambda_1}\left[\left[f''(0) - \frac{f'(0)}{K} + \lambda\left(f'(0)f''(0) - \frac{1}{K^2}[f'(0)]^2\right)\right]\right], \tag{26}$$

$$Nu(\mathrm{Re}_x)^{-1/2} = -\theta'(0), \tag{27}$$

where local Reynolds number is defined as $\mathrm{Re}_x = cx^2 / \nu$.

3. Homotopic solutions

3.1. Zeroth-order deformation problems

Auxiliary functions $\mathbf{H}_f$, $\mathbf{H}_\theta$ and $\mathbf{H}_\Phi$, linear operators L_1, L_2 and L_3 and the initial guesses $f_0(\xi)$, $\theta_0(\xi)$ and $\Phi_0(\xi)$ are taken in the forms

$$\mathbf{H}_f = e^{-2\xi},\ \mathbf{H}_\theta = e^{-2\xi},\ \mathbf{H}_\Phi = e^{-2\xi}, \tag{28}$$

$$L_1 = f^{iv} - 5f'' + 4f,\ L_2 = \theta'' - \theta,\ L_3 = \Phi'' - \Phi, \tag{29}$$

$$f_0(\xi) = e^{-\xi} - e^{-2\xi},\ \theta_0(\xi) = \frac{\gamma_1}{1+\gamma_1}e^{-\xi},\ \Phi_0(\xi) = 1 - \frac{1}{2}e^{-k_2\xi}, \tag{30}$$

subject to the properties

$$L_1[c_1e^{\xi} + c_2e^{-\xi} + c_3e^{2\xi} + c_4e^{-2\xi}] = 0, \tag{31}$$

$$L_2[c_5e^{\xi} + c_6e^{-\xi}] = 0, \tag{32}$$

$$L_3[c_7e^{\xi} + c_8e^{-\xi}] = 0, \tag{33}$$

in which c_i (i = 1–8) are the constants.

If $\hbar_f$, $\hbar_\theta$ and $\hbar_\Phi$ are nonzero auxiliary parameters and $p \in [0,1]$ denotes embedding parameter then the zeroth order deformation problems are as follows:

$$(1-p)L_1[F(\xi;p)-f_0(\xi)] = p\hbar_f \mathbf{H}_f N_f[F(\xi;p)], \tag{34}$$

$$(1-p)L_2[\Theta(\xi;p)-\theta_0(\xi)] = p\hbar_\theta \mathbf{H}_\theta N_\theta[\Theta(\xi;p),\, F(\xi;p)], \tag{35}$$

$$(1-p)L_3[\phi(\xi;p)-\Phi_0(\xi)] = p\hbar_\Phi \mathbf{H}_\Phi N_\Phi[\phi(\xi;p),\, F(\xi;p)], \tag{36}$$

$$\begin{aligned} &F'(0;p)=1,\ F(0;p)=0,\ \Theta'(0;p)=-\gamma_1[1-\Theta(0;p)],\ \phi'(0;p)=k_2\phi(0;p),\\ &F'(\infty;p)=0,\ F''(\infty;p)=0,\ \Theta(\infty;p)=0,\ \phi(\infty,p)=1. \end{aligned} \tag{37}$$

Nonlinear operators are

$$\begin{aligned} N_f = {} & \frac{\partial^4 F(\xi;p)}{\partial\xi^4} + \frac{2}{\xi+K}\frac{\partial^3 F(\xi;p)}{\partial\xi^3} + \frac{1}{(\xi+K)^3}\frac{\partial F(\xi;p)}{\partial\xi} - \frac{1}{(\xi+K)^2}\frac{\partial^2 F(\xi;p)}{\partial\xi^2} \\ & + \lambda\frac{K}{\xi+K}\left(2\frac{\partial^2 F(\xi;p)}{\partial\xi^2}\frac{\partial^3 F(\xi;p)}{\partial\xi^3} - \frac{\partial F(\xi;p)}{\partial\xi}\frac{\partial^4 F(\xi;p)}{\partial\xi^4} - F(\xi;p)\frac{\partial^5 F(\xi;p)}{\partial\xi^5}\right. \\ & + \frac{3}{(\xi+K)^3}F(\xi;p)\frac{\partial^2 F(\xi;p)}{\partial\xi^2} - \frac{1}{(\xi+K)^2}F(\xi;p)\frac{\partial^3 F(\xi;p)}{\partial\xi^3} + \frac{3}{(\xi+K)^3}\left(\frac{\partial F(\xi;p)}{\partial\xi}\right)^2 \\ & \left. - \frac{3}{(\xi+K)^4}F(\xi;p)\frac{\partial F(\xi;p)}{\partial\xi} - \frac{3}{(\xi+K)^2}\frac{\partial F(\xi;p)}{\partial\xi}\frac{\partial^2 F(\xi;p)}{\partial\xi^2}\right) + (1+\lambda_1)\frac{K}{\xi+K} \\ & + \left(F(\xi;p)\frac{\partial^3 F(\xi;p)}{\partial\xi^3} - \frac{\partial F(\xi;p)}{\partial\xi}\frac{\partial^2 F(\xi;p)}{\partial\xi^2}) + \frac{1}{\xi+K}F(\xi;p)\frac{\partial^2 F(\xi;p)}{\partial\xi^2}\right. \\ & \left. - \frac{1}{\xi+K}\left(\frac{\partial F(\xi;p)}{\partial\xi}\right)^2 - \frac{1}{(\xi+K)^2}F(\xi;p)\frac{\partial F(\xi;p)}{\partial\xi} - M\frac{\partial^2 F(\xi;p)}{\partial\xi^2} - \frac{M}{\xi+K}\frac{\partial F(\xi;p)}{\partial\xi}\right), \end{aligned} \tag{38}$$

$$N_\theta = \frac{1}{\mathrm{Pr}}\left(\frac{\partial^2\Theta(\xi;p)}{\partial\xi^2} + \frac{1}{\xi+K}\frac{\partial\Theta(\xi;p)}{\partial\xi}\right) + \frac{K}{\xi+K}F(\xi;p)\frac{\partial\Theta(\xi;p)}{\partial\eta}, \tag{39}$$

$$\begin{aligned} N_\Phi = {} & \frac{1}{Sc}\left(\frac{\partial^2\phi(\xi;p)}{\partial\xi^2} + \frac{1}{\xi+K}\frac{\partial\phi(\xi;p)}{\partial\xi}\right) + \frac{K}{\xi+K}F(\xi;p)\frac{\partial\phi(\xi;p)}{\partial\xi} \\ & - k_1\phi(\xi;p)(1-\phi(\xi;p))^2. \end{aligned} \tag{40}$$

3.2. mth-order deformation problems

The mth order deformation problems are

$$L_1[f_m - \chi_m f_{m-1}] = \hbar_f \mathbf{R}_m^f, \tag{41}$$

$$L_2[\theta_m - \chi_m \theta_{m-1}] = \hbar_\theta \mathbf{R}_m^\theta, \tag{42}$$

$$L_3[\Phi_m - \chi_m \Phi_{m-1}] = \hbar_\Phi \mathbf{R}_m^\Phi, \tag{43}$$

$$\begin{aligned} &\left.\frac{\partial f_m}{\partial \xi}\right|_{\xi=0} = f_m\Big|_{\xi=0} = \left.\frac{\partial f_m}{\partial \xi}\right|_{\xi\to\infty} = 0, \\ &\left.\frac{\partial \theta_m}{\partial \xi}\right|_{\xi=0} - \gamma_1 \theta_m\Big|_{\xi=0} = \theta_m\Big|_{\xi\to\infty} = 0, \\ &\left.\frac{\partial \Phi_m}{\partial \xi}\right|_{\xi=0} - k_2 \Phi_m\Big|_{\xi=0} = \Phi_m\Big|_{\xi\to\infty} = 0, \end{aligned} \tag{44}$$

$$\begin{aligned} \mathbf{R}_m^f = {} & f_{m-1}^{iv} + \frac{2}{\xi+K} f_{m-1}''' + \frac{1}{(\xi+K)^3} f_{m-1}' - \frac{1}{(\xi+K)^2} f_{m-1}'' + \lambda \sum_{k=0}^{m-1} \left(\frac{2K}{\xi+K} f_{m-1-k}'' f_k''' \right. \\ & - \frac{K}{\xi+K} f_{m-1-k}' f_k^{iv} - \frac{K}{\xi+K} f_{m-1-k} f_k^{v} + \frac{3K}{(\xi+K)^4} f_{m-1-k} f_k'' - \frac{K}{(\xi+K)^3} f_{m-1-k} f_k''' \\ & \left. - \frac{3K}{(\xi+K)^3} f_{m-1-k}' f_k'' - \frac{3K}{(\xi+K)^5} f_{m-1-k} f_k' + \frac{3K}{(\xi+K)^4} f_{m-1-k}' f_k' \right) + (1+\lambda_1) \\ & \left[\frac{K}{\xi+K} \sum_{k=0}^{m-1} \left(f_{m-1-k} f_k''' - f_{m-1-k}' f_k'' + \frac{1}{\xi+K} (f_{m-1-k} f_k'' - f_{m-1-k}' f_k') - \frac{1}{(\xi+K)^2} f_{m-1-k} f_k' \right) \right. \\ & \left. - M f_{m-1}'' - \frac{M}{\xi+K} f_{m-1}' \right], \end{aligned} \tag{45}$$

$$\mathbf{R}_m^\theta = \frac{1}{\mathrm{Pr}} \left(\theta_{m-1}'' + \frac{1}{\xi+K} \theta_{m-1}' \right) + \frac{K}{\xi+K} \sum_{k=0}^{m-1} f_{m-1-k} \theta_k', \tag{46}$$

$$\begin{aligned} \mathbf{R}_m^\Phi = {} & \frac{1}{Sc} \left(\Phi_{m-1}'' + \frac{1}{\xi+K} \Phi_{m-1}' \right) + \frac{K}{\xi+K} \sum_{k=0}^{m-1} f_{m-1-k} \Phi_k' \\ & - k_1 \sum_{k=0}^{m-1} \left(\Phi_{m-1-l} \sum_{j=0}^{l} \Phi_{l-j} \Phi_j - 2\Phi_{m-1-l} \Phi_l \right) - k_1 \Phi_{m-1}, \end{aligned} \tag{47}$$

$$\chi_m = \begin{cases} 0, & m \le 1 \\ 1, & m > 1 \end{cases}. \tag{48}$$

The general solutions (f_m, θ_m, Φ_m) comprising the special solutions $(f_m^*, \theta_m^*, \Phi_m^*)$ are

$$f_m(\xi) = f_m^*(\xi) + c_1 e^{\xi} + c_2 e^{-\xi} + c_3 e^{2\xi} + c_4 e^{-2\xi}, \tag{49}$$

$$\theta_m(\xi) = \theta_m^*(\xi) + c_5 e^{\xi} + c_6 e^{-\xi}, \tag{50}$$

$$\Phi_m(\xi) = \Phi_m^*(\xi) + c_7 e^{\xi} + c_8 e^{-\xi}, \tag{51}$$

where the constants c_i (i = 1–8) through the boundary conditions (44) have the values

$$\begin{aligned} &c_1 = c_3 = c_5 = c_7 = 0,\ c_2 = -c_4 - f_m^*(0),\ c_4 = \left.\frac{\partial \theta_m^*(\xi)}{\partial \xi}\right|_{\xi=0} + f_m^*(0), \\ &c_6 = \frac{1}{1+\gamma_1}\left[\left.\frac{\partial \theta_m^*(\xi)}{\partial \xi}\right|_{\xi=0} - \gamma_1 \theta_m^*(0)\right],\ c_8 = \frac{1}{1+k_2}\left[\left.\frac{\partial \Phi_m^*(\xi)}{\partial \xi}\right|_{\xi=0} - k_2 \Phi_m^*(0)\right]. \end{aligned} \tag{52}$$

4. Convergence analysis

Homotopy analysis method (HAM) involves an embedding auxiliary parameter $\hbar$ which gives the freedom to choose and adjust convergence region of series solutions. The $\hbar$–curves are plotted to obtain valid ranges of these parameters (see Fig 1). Allowed values of $\hbar_f$, $\hbar_\theta$ and $\hbar_\Phi$ are $-1.7 \leq \hbar_f \leq -0.9$, $-2 \leq \hbar_\theta \leq -0.2$ and $-0.7 \leq \hbar_\Phi \leq -0.3$. Also HAM solutions converge when $\hbar_f = -0.9$, $\hbar_\theta = -1$ and $\hbar_\Phi = -0.3$ (Table 1).

5. Results and Discussion

In this section the effects of different parameters on the velocity, temperature and concentration fields are investigated through plots.

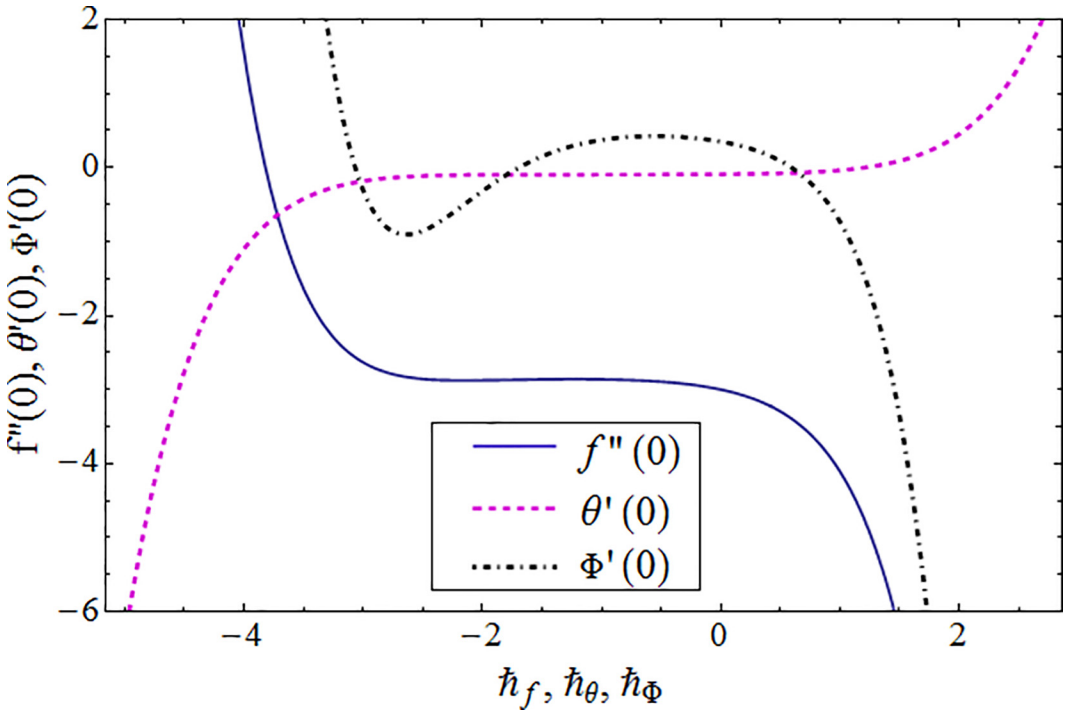

Fig 1. The $\hbar$–curves for $f''(0)$, $\theta'(0)$ and $\Phi'(0)$ when $K = 0.01$, $\lambda_1 = 0.5$, $\lambda = 0.9$, $\gamma_1 = 0.1$, $M = 0.3$, Pr = 1, $Sc = k_1 = 0.9$ and $k_2 = 0.7$.

doi:10.1371/journal.pone.0161641.g001

Table 1. HAM solutions convergence when $K = 0.01$, $\lambda_1 = 0.5$, $\lambda = 0.9$, $\gamma_1 = 0.1$, $M = 0.3$, $Pr = 1$, $Sc = k_1 = 0.9$ and $k_2 = 0.7$.

Order of approximations	$-f''(0)$	$-\theta'(0)$	$\Phi'(0)$
1	12.956	0.09395	0.3557
5	2.879	0.09867	0.3773
8	2.865	0.09924	0.3925
10	2.865	0.09931	0.4022
15	2.865	0.09939	0.4167
20	2.865	0.09939	0.4179
26	2.865	0.09939	0.4184
30	2.865	0.09939	0.4184

doi:10.1371/journal.pone.0161641.t001

5.1. Dimensionless velocity profile

Fig 2 depicts the variation of Hartman number M on the velocity distribution $f'(\xi)$. An enhancement in the strength of magnetic field produces a resistive force which signifies the reduction of the fluid velocity. Here negative values of $f'(\xi)$ indicate downward flow in the vertical direction. Fig 3 illustrates the behavior of Deborah number λ on the horizontal component of velocity $f'(\xi)$. An increase in retardation time enhances elasticity. Since elasticity and viscosity effects are inversely proportional to each other so decrease in viscosity enhances the fluid velocity. Impact of λ_1 on velocity profile $f'(\xi)$ is depicted in Fig 4. An increase in λ_1 corresponds to increase in relaxation time. It means particle needs much more time to come back from perturbed system to equilibrium system and consequently the fluid velocity decreases. Fig 5 shows impact of curvature parameter K on the velocity profile $f'(\xi)$. Here increment in the magnitude of velocity profile is subjected to the enhanced values of K.

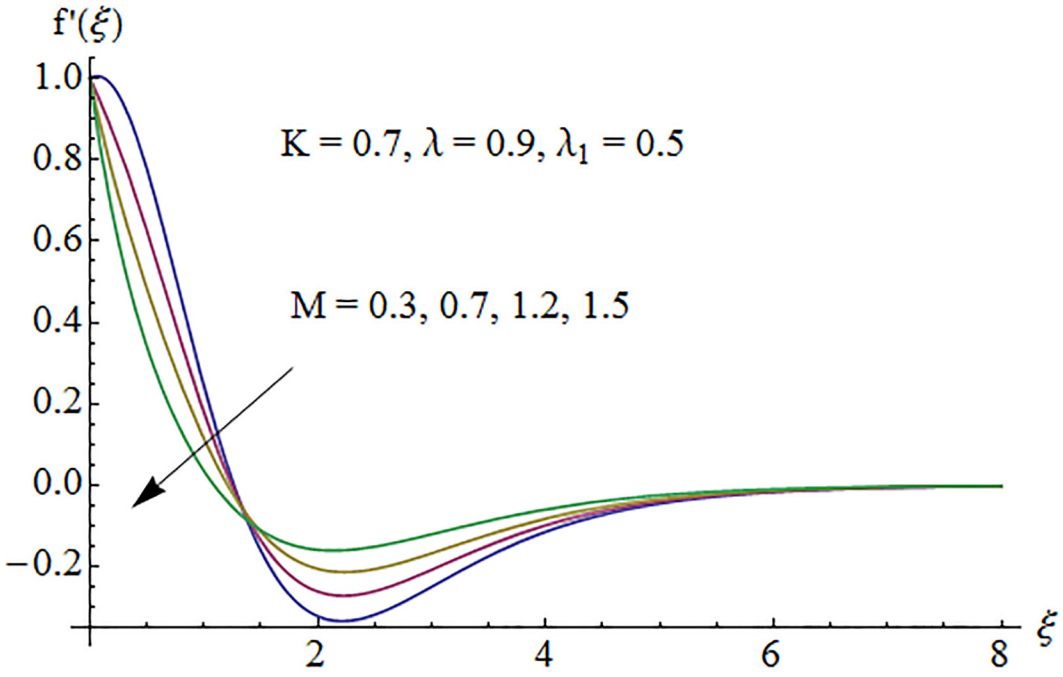

Fig 2. Impact of M on velocity.

doi:10.1371/journal.pone.0161641.g002

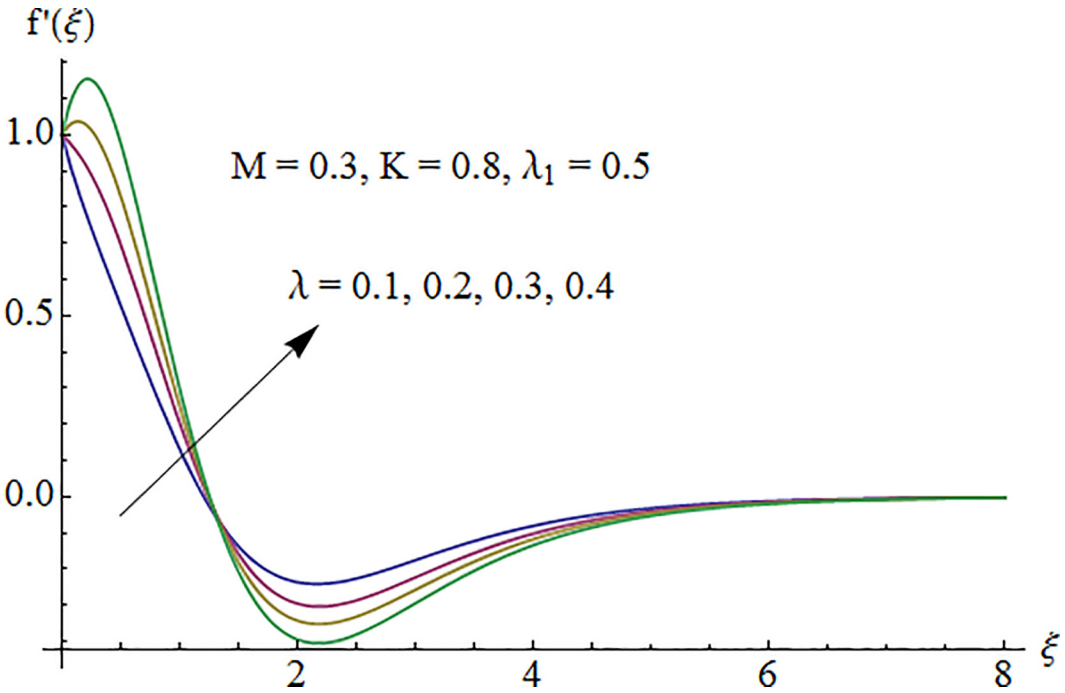

Fig 3. Impact of λ on velocity.

doi:10.1371/journal.pone.0161641.g003

5.2. Dimensionless temperature profile

Temperature profile $\theta(\xi)$ is plotted in Fig 6 to show the effect of Prandtl number Pr. Since the thermal diffusivity decreases by increasing Pr so the temperature decreases. Fig 7 indicates that

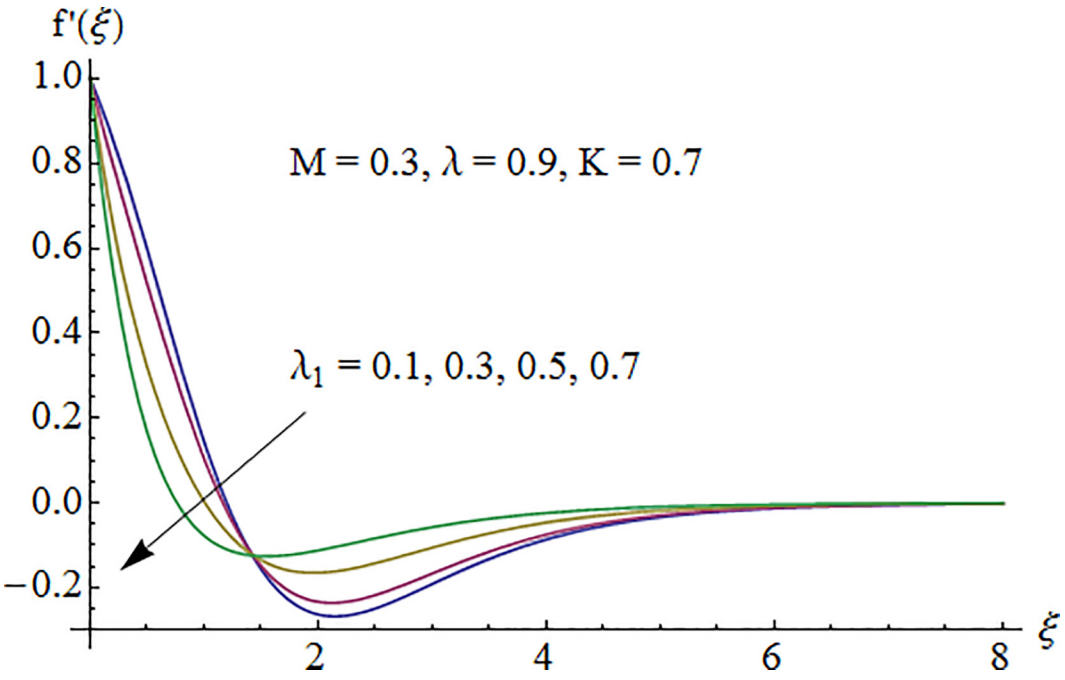

Fig 4. Impact of λ_1 on velocity.

doi:10.1371/journal.pone.0161641.g004

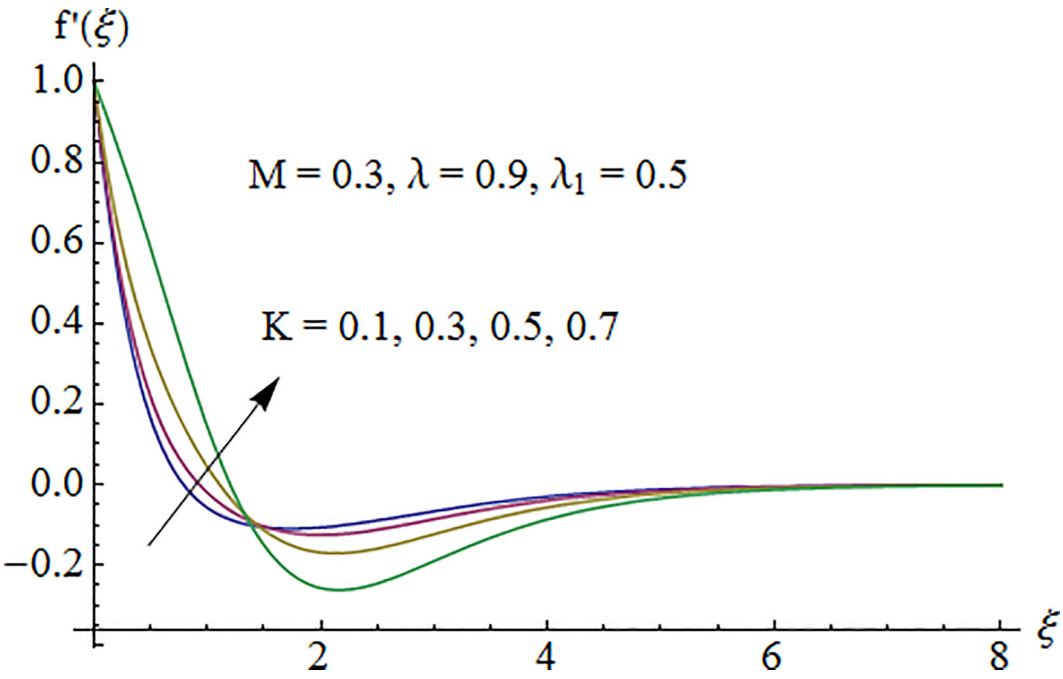

Fig 5. Impact of *K* on velocity.

doi:10.1371/journal.pone.0161641.g005

temperature increases for larger thermal Biot number γ_1 as convective heat transfer coefficient enhances through increasing thermal Biot number γ_1. Fig 8 exhibits variation of curvature parameter K on the dimensionless temperature profile $\theta(\xi)$. Enhancement in temperature distribution is observed for larger values of K.

5.3. Dimensionless concentration profile

Fig 9 shows that concentration profile $\Phi(\xi)$ is decreasing function of Schmidt number Sc. As increase in Sc reduces the mass diffusivity which consequently decrease fluid concentration. Fig 10 depicts the effect of strength of homogeneous reaction parameter k_1 on concentration profile. Fluid concentration decreases due to the consumption of reactants when k_1 is enhanced. Variation of strength of heterogeneous reaction parameter k_2 on Φ is portrayed in Fig 11. Here the concentration profile increases for larger k_2.

5.4 Dimensionless pressure profile

Figs 12–14 elucidate the variation in pressure profile for increasing values of Deborah number λ, ratio of relaxation to retardation times λ_1 and curvature parameter K. Here an enhancement in pressure distribution is noted for increasing λ. Also pressure is decreasing function of λ_1 and K.

5.5 Skin friction coefficient

Fig 15 shows variation of curvature parameter K on surface drag force $\frac{1}{2}C_f(\mathrm{Re}_x)^{1/2}$ against Hartman number M. It is noted that skin friction coefficient enhances for larger K and it reduces when M is increased. Impact of ratio of relaxation to retardation times λ_1 via Deborah number λ on surface drag force is illustrated in Fig 16. Here surface drag force decreases for increasing λ_1 while it increases for larger λ. Computed results of skin friction coefficient are compared with previously published articles in limiting cases and found in very good agreement (see Table 2).

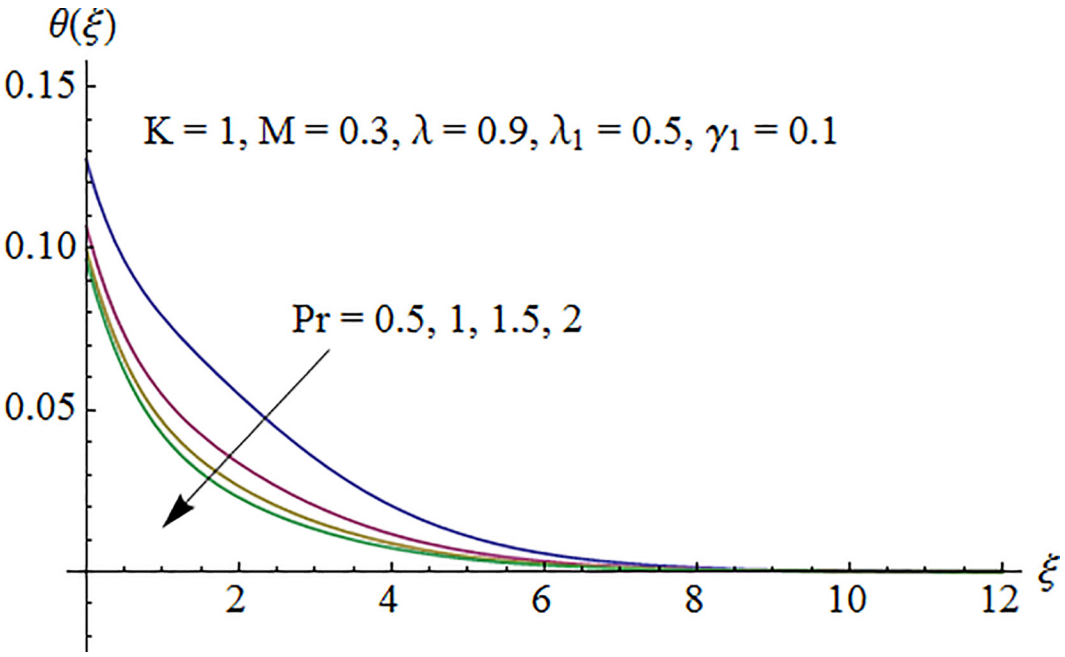

Fig 6. Impact of Pr on temperature.

doi:10.1371/journal.pone.0161641.g006

5.6 Nusselt number

Impact of Biot number λ_1 on surface heat transfer rate $Nu(\mathrm{Re}_x)^{-1/2}$ via Prandtl number Pr is shown in Fig 17. It is noted that heat transfer rate enhances for larger values of λ_1 and Pr. Fig 18 illustrates variation of Prandtl number Pr on Nusselt number against curvature parameter

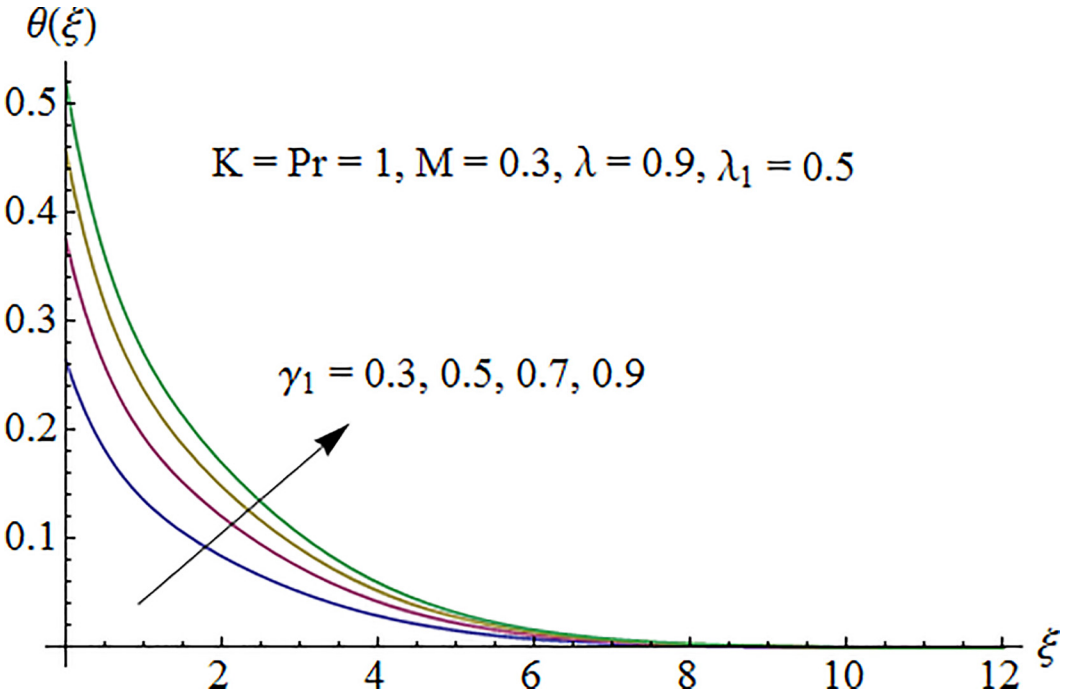

Fig 7. Impact of γ_1 on temperature.

doi:10.1371/journal.pone.0161641.g007

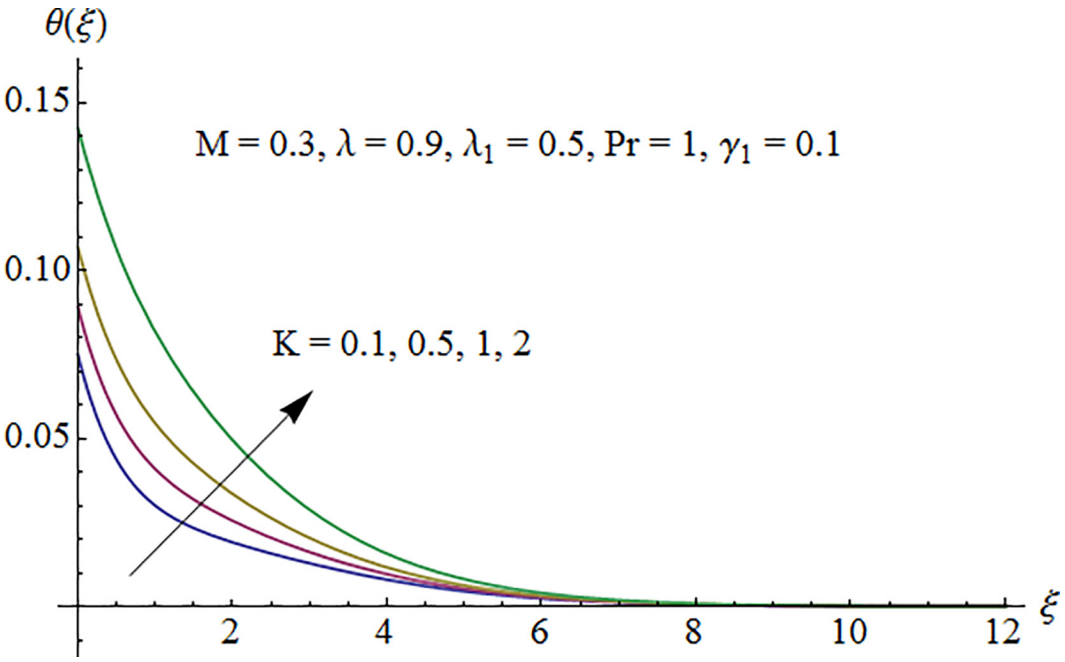

Fig 8. Impact of *K* on temperature.

doi:10.1371/journal.pone.0161641.g008

K. Here surface heat transfer rate decreases as curvature parameter *K* is enhanced while opposite effect is observed for increasing Pr.

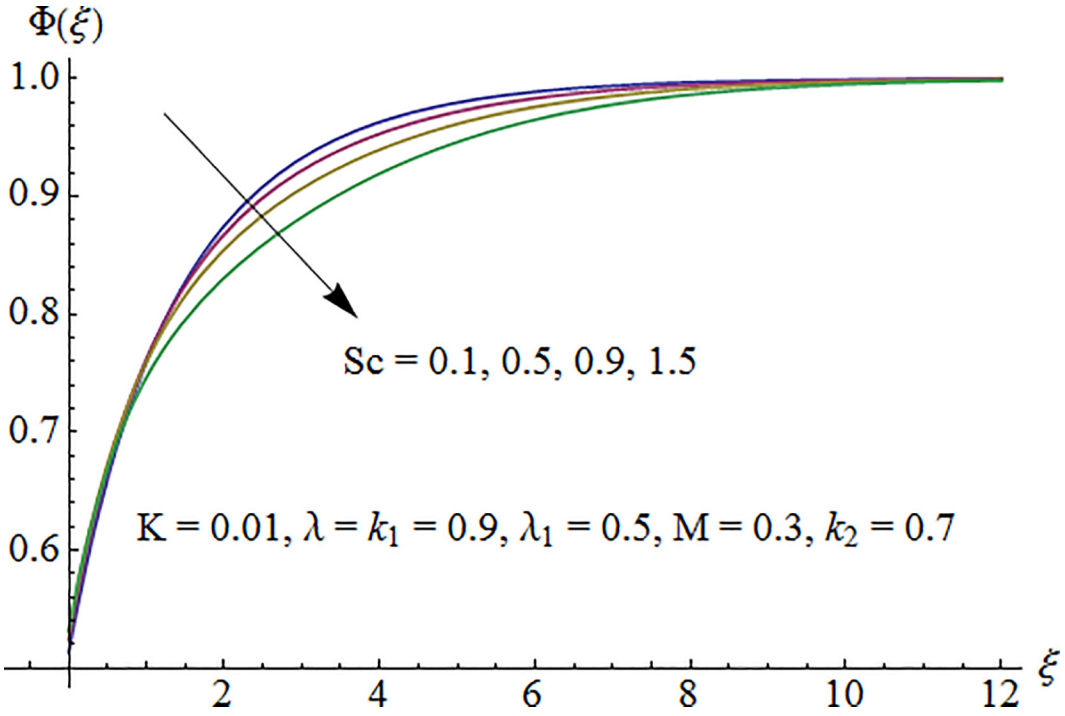

Fig 9. Impact of *Sc* on concentration.

doi:10.1371/journal.pone.0161641.g009

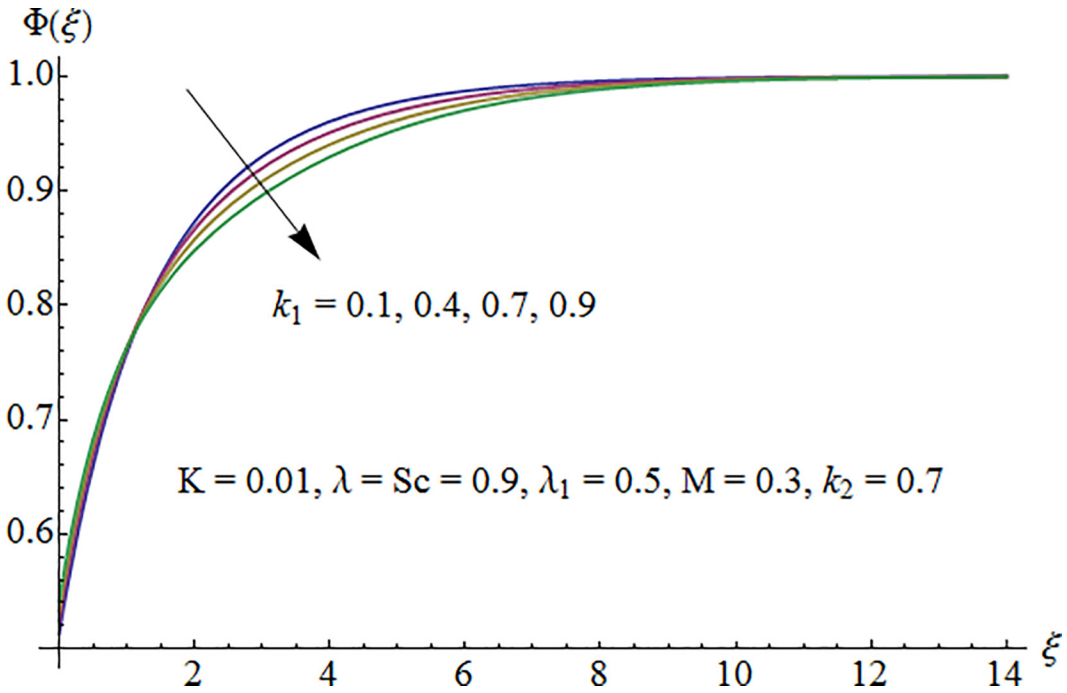

Fig 10. Impact of k_1 on concentration.

doi:10.1371/journal.pone.0161641.g010

5.7 Surface concentration

Variation of homogeneous reaction parameter k_1 on surface concentration $\Phi(0)$ against Schmidt number *Sc* is shown in Fig 19. One can see that surface concentration decreases with the increase of k_1 and *Sc*. It is in view of the fact that surface concentration reduces due to the

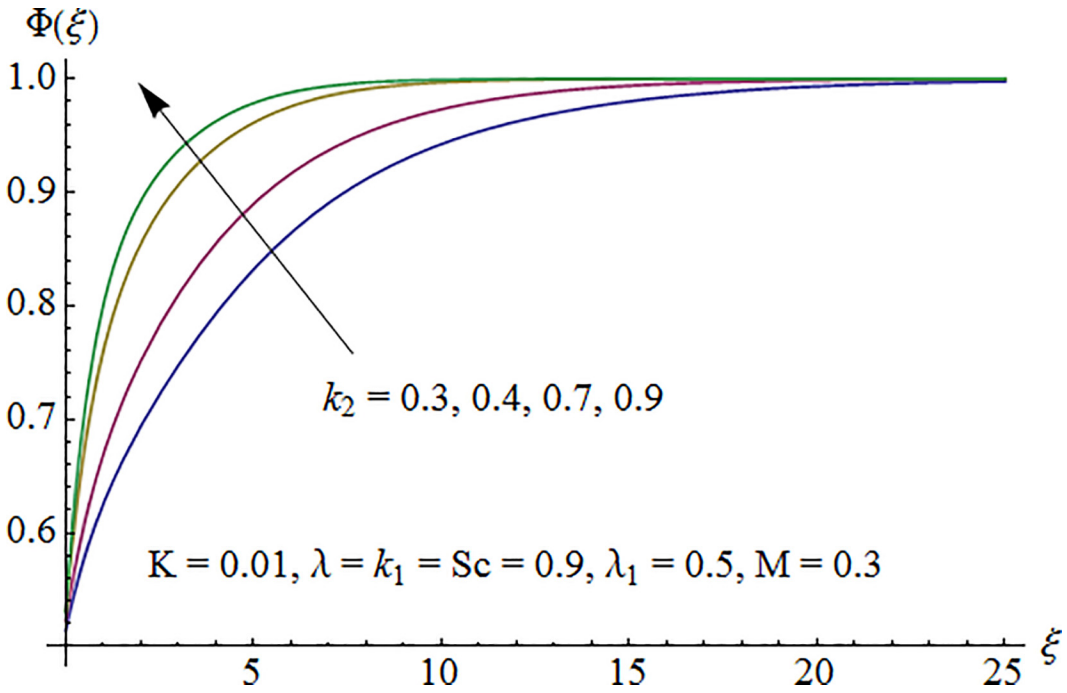

Fig 11. Impact of k_2 on concentration.

doi:10.1371/journal.pone.0161641.g011

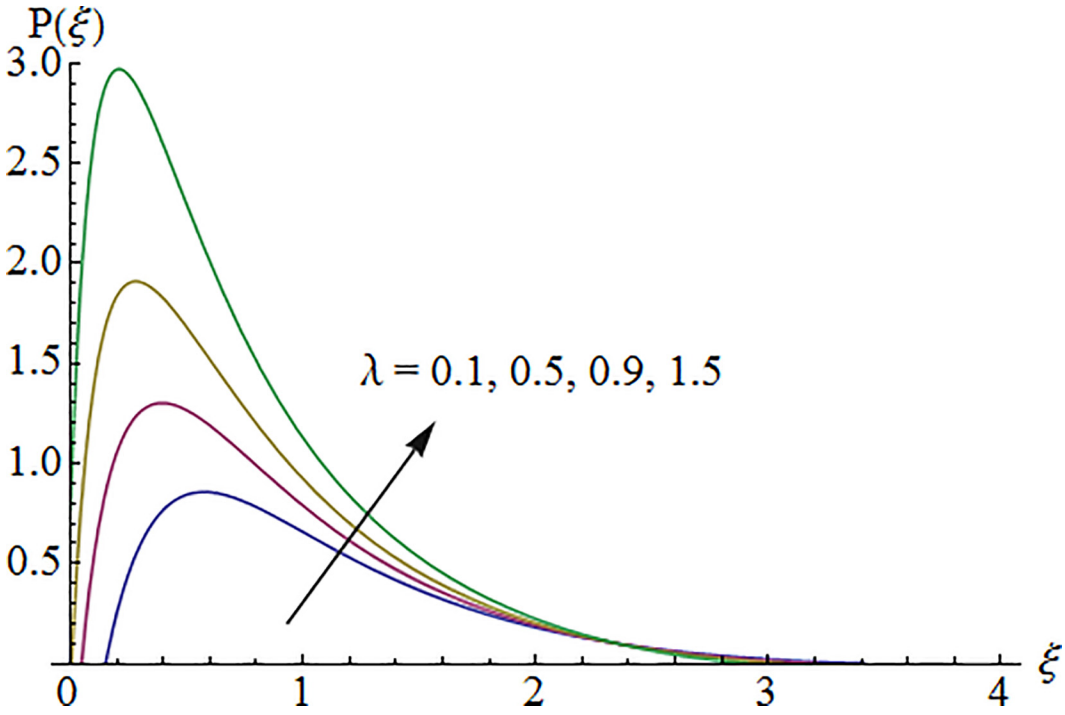

Fig 12. Impact of λ on pressure.

doi:10.1371/journal.pone.0161641.g012

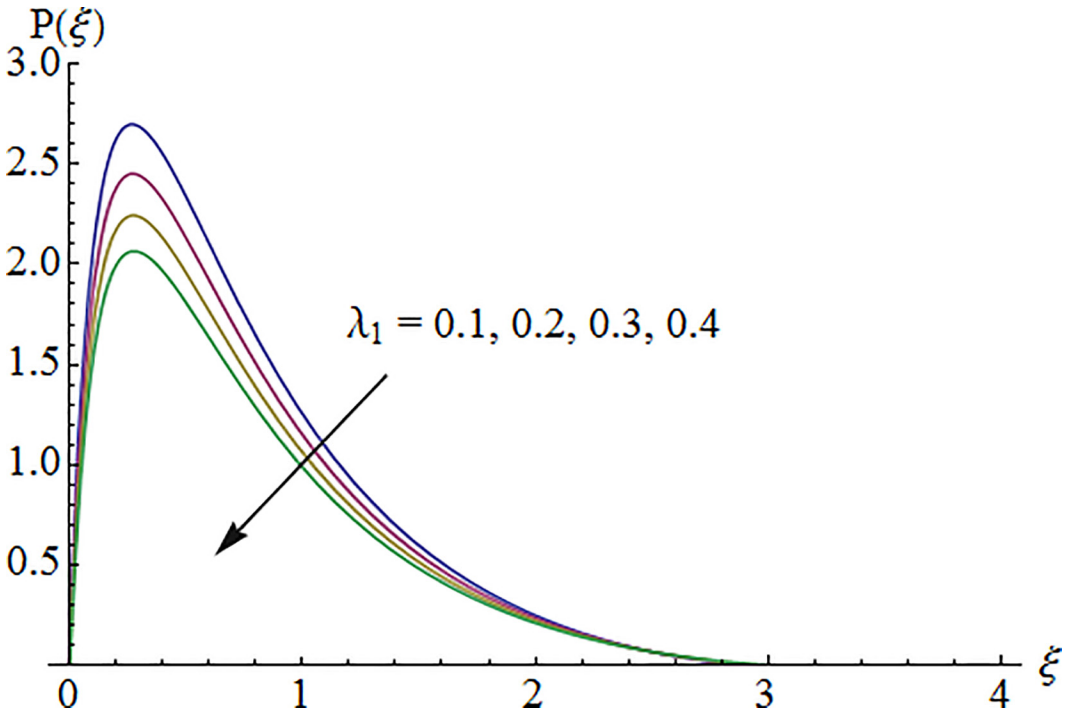

Fig 13. Impact of λ_1 on pressure.

doi:10.1371/journal.pone.0161641.g013

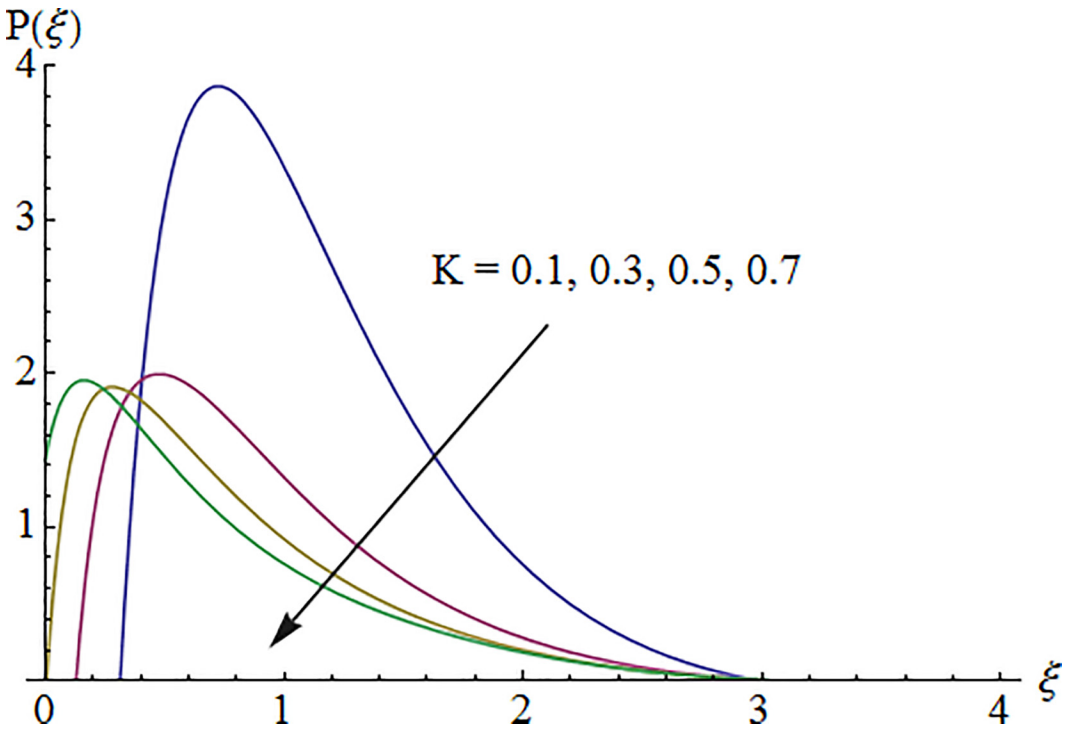

Fig 14. Impact of *K* on pressure.

doi:10.1371/journal.pone.0161641.g014

consumption of reactants during chemical reaction. Influence of surface concentration via Schmidt number *Sc* for higher heterogeneous reaction parameter k_2 is depicted in Fig 20. Here surface concentration increases when k_2 is enhanced.

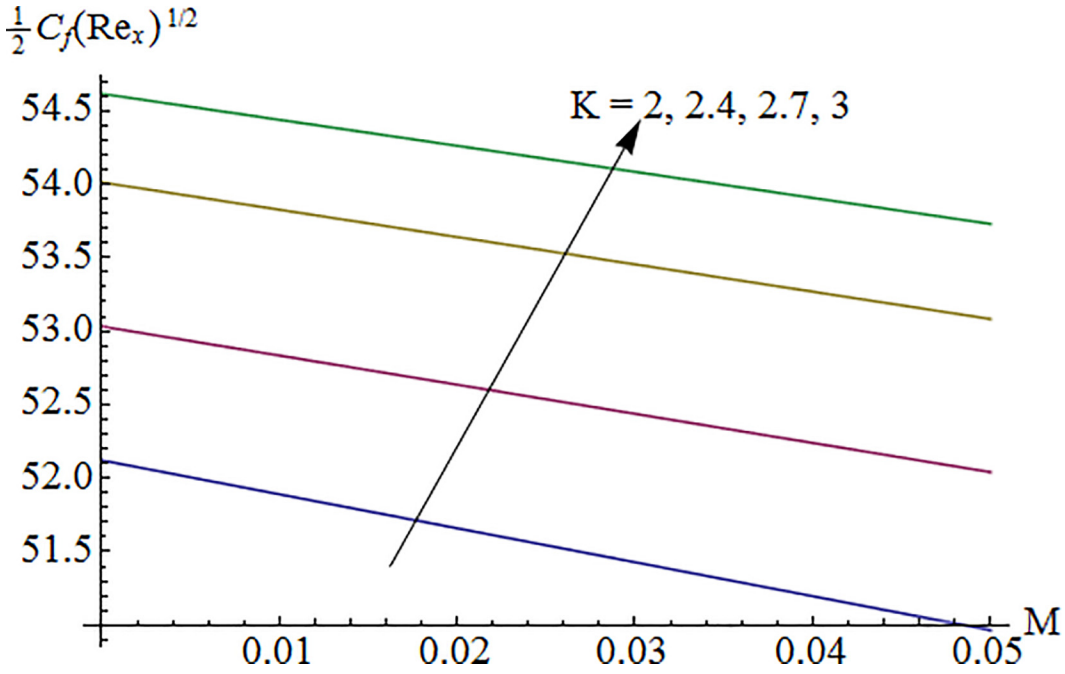

Fig 15. Impact of *K* via *M* on $\frac{1}{2}C_f(\mathrm{Re}_x)^{1/2}$.

doi:10.1371/journal.pone.0161641.g015

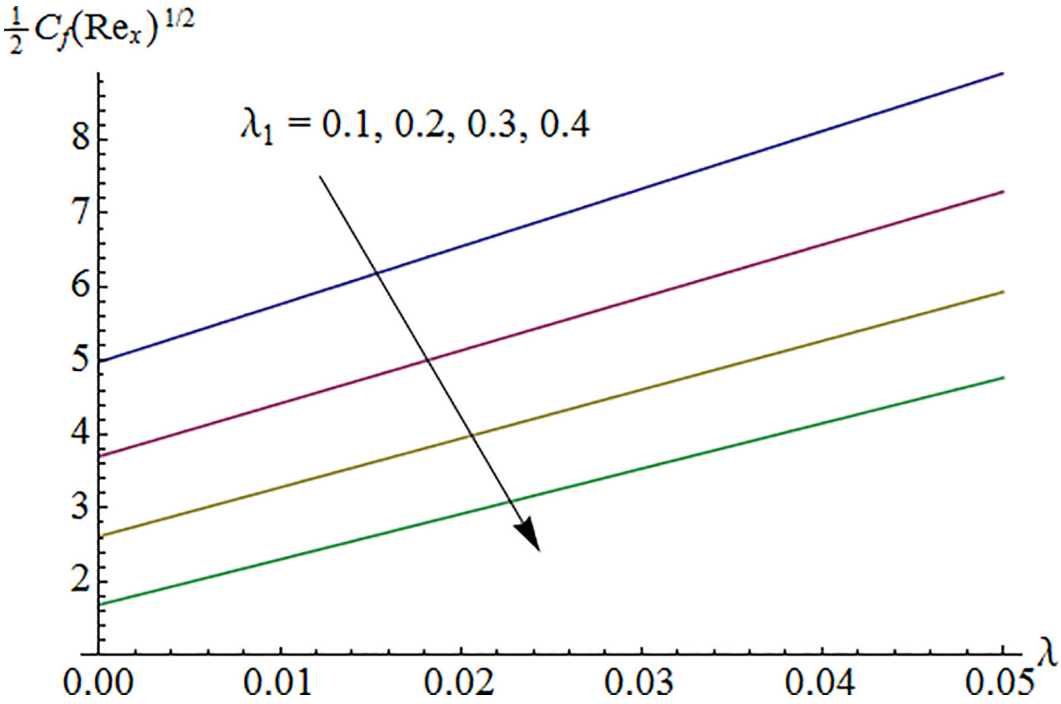

Fig 16. Impact of λ_1 via λ on $\frac{1}{2}C_f(\mathrm{Re}_x)^{1/2}$.

doi:10.1371/journal.pone.0161641.g016

6. Concluding Remarks

Effects of homogeneous—heterogeneous reactions in convective flow of Jeffrey fluid due to a curved stretching sheet are studied. The following outcomes are noticed:

- Increase in the values of Deborah number and curvature parameter has similar effects on the velocity in a qualitative sense
- Fluid velocity and temperature enhance for larger curvature parameter.
- The strength of heterogeneous reaction enhances the fluid concentration.
- Pressure distribution has direct relationship with Deborah number.
- Opposite behavior of curvature parameter and Hartman number is seen on the surface drag force.
- Increasing values of Biot number correspond to an enhancement in temperature and Nusselt number.

Table 2. Comparison of skin friction coefficient $\frac{1}{2}C_f(\mathrm{Re}_x)^{1/2}$. with previous published articles when $\lambda_1 = 0 = \lambda$ and $K = \infty$.

M	Hayat et al. [43]	Mabood and Das [44]	Present
1	1.4142	1.4142135	1.4142
5	2.4494	2.4494897	2.4494
10	3.31662	3.31662	3.3166
50	7.14142	7.1414284	7.1414

doi:10.1371/journal.pone.0161641.t002

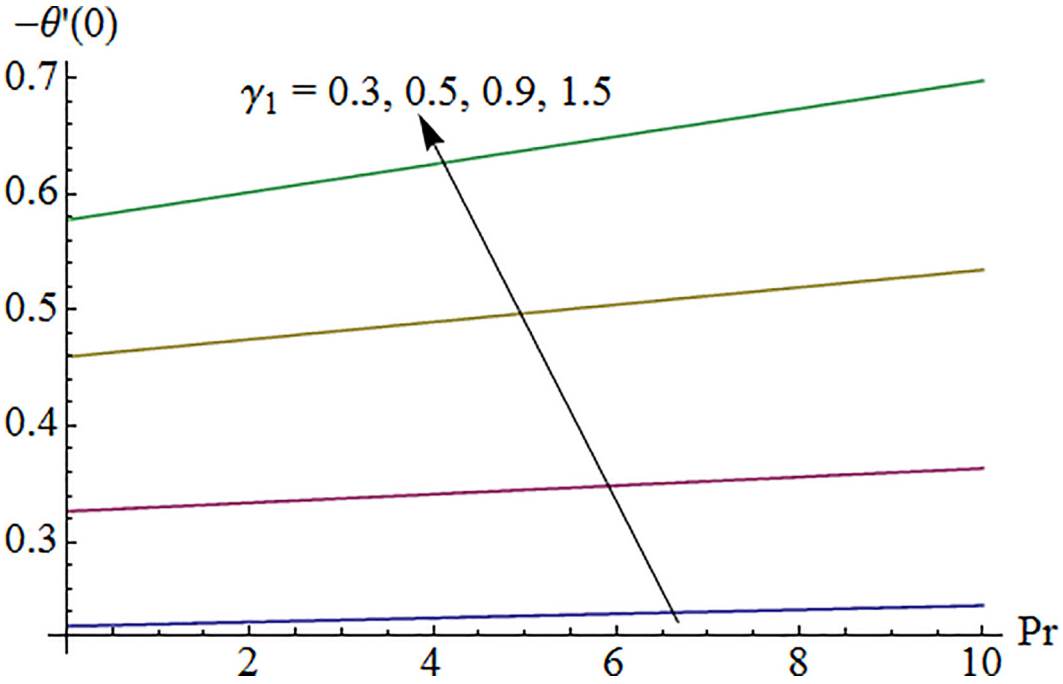

Fig 17. Impact of γ_1 via Pr on $-\theta'(0)$.

doi:10.1371/journal.pone.0161641.g017

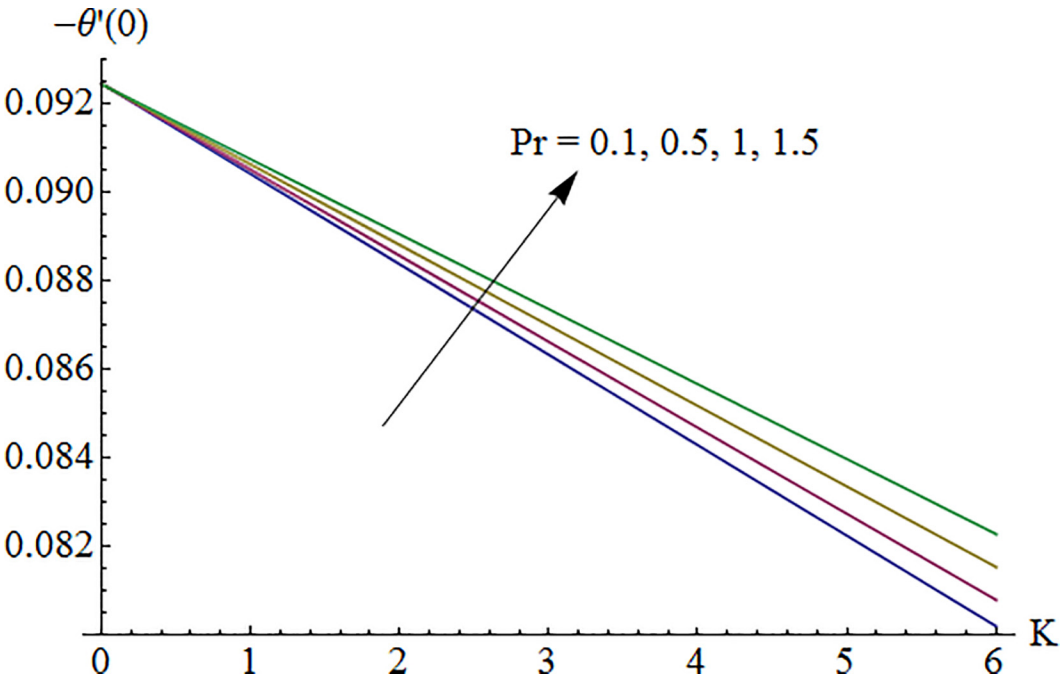

Fig 18. Impact of Pr via K on $-\theta'(0)$.

doi:10.1371/journal.pone.0161641.g018

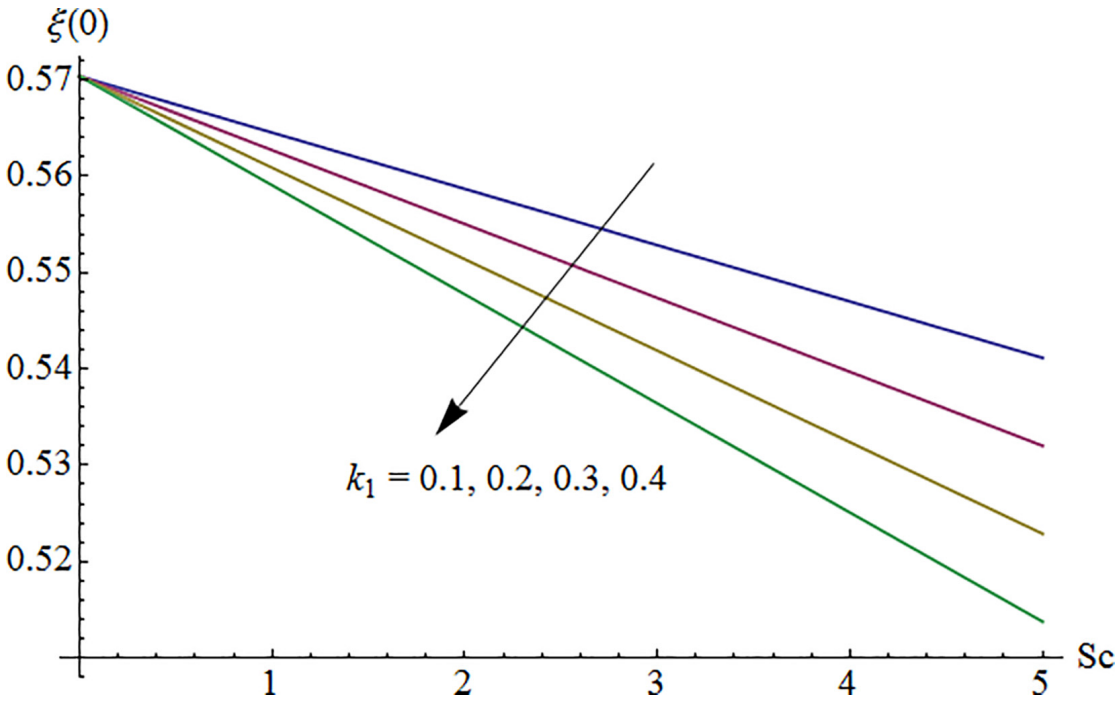

Fig 19. Impact of k_1 via *Sc* on Φ(0).

doi:10.1371/journal.pone.0161641.g019

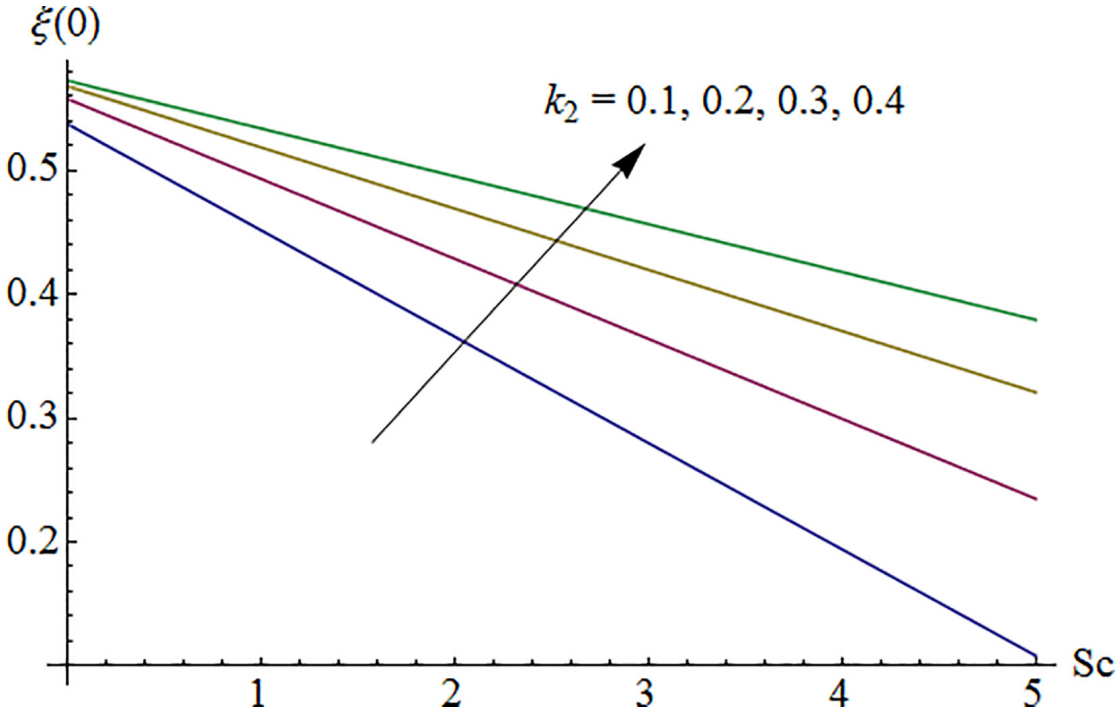

Fig 20. Impact of k_2 via *Sc* on Φ(0).

doi:10.1371/journal.pone.0161641.g020

Author Contributions

Conceptualization: MI TH AA.

Data curation: MI TH AA.

Formal analysis: MI TH AA.

Investigation: MI TH AA.

Methodology: MI TH AA.

Project administration: MI TH AA.

Resources: MI TH AA.

Software: MI TH AA.

Supervision: MI TH AA.

Validation: MI TH AA.

Visualization: MI TH AA.

Writing – original draft: MI TH AA.

Writing – review & editing: MI TH AA.

References

1. Tripathi D, Ali N, Hayat T, Chaube MK, Hendi AA (2011) Peristaltic flow of MHD Jeffrey fluid through a finite length cylindrical tube. Appl MathMech (Eng Ed) 32, 1148–1160.
2. Das K (2012) Influence of slip and heat transfer on MHD peristaltic flow of a Jeffrey fluid in an inclined asymmetric porous channel. Ind J Math 54, 19–45.
3. Hamad MAA, Gaied SMA, Khan WA (2013) Thermal jump effects on boundary layer flow of a Jeffrey fluid near the stagnation point on a stretching/shrinking sheet with variable thermal conductivity. J Fluids 2013, 749271.
4. Shehzad SA, Hayat T, Alsaedi A, Obid MA (2014) Nonlinear thermal radiation in three-dimensional flow of Jeffrey nanofluid: A model for solar energy. Appl Math Comp 248, 273–286.
5. Ellahi R, Hussain F (2015) Simultaneous effects of MHD and partial slip on peristaltic flow of Jeffrey fluid in a rectangular duct. J Magn Magn Mater 393, 284–292.
6. Hayat T, Imtiaz M Alsaedi A (2015) Magnetohydrodynamic stagnation point flow of a Jeffrey nanofluid with Newtonian heating. J Aerospace Eng doi: 10.1061/(ASCE)AS.1943-5525.0000568,04015063
7. Reddy GB, Sreenadh S, Reddy RH, Kavitha A (2015) Flow of a Jeffrey fluid between torsionally oscillating disks, Ain Shams Eng J 6, 355–362.
8. Farooq M, Gull N, Alsaedi A Hayat T (2015) MHD flow of a Jeffrey fluid with Newtonian heating. J Mech 33, 1–11.
9. Merkin JH (1996) A model for isothermal homogeneous-heterogeneous reactions in boundary layer flow. Math Comp Model 24, 125–136.
10. Chaudhary MA, Merkin JH (1995) A simple isothermal model for homogeneous-heterogeneous reactions in boundary layer flow: I. Equal diffusivities. Fluid DynRes 16,311–333.
11. Bachok N, Ishak A, Pop I (2011) On the stagnation-point flow towards a stretching sheet with homogeneous—heterogeneous reactions effects Commun Nonlinear Sci Numer Simul 16, 4296–4302.
12. Khan WA, Pop I (2012) Effects of homogeneous-heterogeneous reactions on the viscoelastic fluid towards a stretching sheet. ASME J Heat Transf 134, 1–5.
13. Shaw S, Kameswaran PK, Sibanda P (2013) Homogeneous-heterogeneous reactions in micropolar fluid flow from a permeable stretching or shrinking sheet in a porous medium. Boundary Value Problems 2013, 77.
14. Kameswaran PK, Shaw S, Sibanda P, Murthy PVSN (2013) Homogeneous-heterogeneous reactions in a nanofluid flow due to porous stretching sheet. Int J Heat Mass Transf 57, 465–472.

15. Hayat T, Imtiaz M, Alsaedi A (2015) Impact of magnetohydrodynamics in bidirectional flow of nanofluid subject to second order slip velocity and homogeneous—heterogeneous reactions. J. Magn Magn Mater 395, 294–302.
16. Hayat T, Imtiaz M, Alsaedi A, Almezal S (2016) On Cattaneo-Christov heat flux in MHD flow of Oldroyd-B fluid with homogeneous-heterogeneous reactions. J. Magn Magn Mater 104, 296–303.
17. Gao ZK, Yang YX, Fang PC, Jin ND, Xia CY, Hu LD (2015) Multi-frequency complex network from time series for uncovering oil-water flow structure Scientific Reports 5, 8222. doi: 10.1038/srep08222 PMID: 25649900
18. Gao ZK, Yang YX, Zhai LS, Ding MS, Jin ND (2016) Characterizing slug to churn flow transition by using multivariate pseudo Wigner distribution and multivariate multiscale entropy. Chem Eng. J. 291, 74–81.
19. Gao ZK, Fang PC, Ding MS, Jin ND (2015) Multivariate weighted complex network analysis for characterizing nonlinear dynamic behavior in two-phase flow. Exp. Thermal Fluid Sci. 60, 157–164.
20. Gao ZK, Yang YX, Zhai LS, Jin ND, Chen G (2016) A four-sector conductance method for measuring and characterizing low-velocity oil-water two-phase flows. IEEE Transactions on Instrume 65, 1690–1697.
21. Crane LJ (1970) Flow past a stretching plate. J. Appl. Math. Phy. (ZAMP) 21, 645–647.
22. Cortell R (2013) Fluid flow and radiative nonlinear heat transfer over stretching sheet. J. King Saud Uni-Sci. 26, 161–167.
23. Hsiao KL (2010) Heat and mass mixed convection for MHD viscoelastic fluid past a stretching sheet with ohmic dissipation. Commun. Nonlinear Sci. Numer. Simul. 15, 1803–1812.
24. Hsiao KL (2010) Corrigendum to Heat and mass mixed convection for MHD viscoelastic fluid past a stretching sheet with Ohmic dissipation [Commun Nonlinear Sci. Numer. Simul. 15 (2010) 1803–1812], Commun. Nonlinear Sci Numer Simul doi: 10.1016/j.cnsns.2015.04.004, 232
25. Hsiao KL (2011) MHD mixed convection for viscoelastic fluid past a porous wedge. Int J Non-Linear Mech 46, 1–8.
26. Malvandi A, Hedayati F, Ganji DD (2014) Slip effects on unsteady stagnation point flow of a nanofluid over a stretching sheet. Powder Tech 253, 377–384.
27. Hsiao KL (2016) Stagnation electrical MHD nanofluid mixed convection with slip boundary on a stretching sheet. Appl Thermal Eng 98, 850–861.
28. Sheikholeslami M, Ganji DD, Javed MY, Ellahi R (2015) Effect of thermal radiation on magnetohydrodynamics nanofluid flow and heat transfer by means of two phase model. J Magn Magn Mater 374, 36–43.
29. Lin Y, Zheng L, Chen G (2015) Unsteady flow and heat transfer of pseudo-plastic nanoliquid in a finite thin film on a stretching surface with variable thermal conductivity and viscous dissipation. Powder Tech 274, 324–332.
30. Sajid M, Ali N, Javed T, Abbas Z (2010) Stretching a curved surface in a viscous fluid. Chinese Phy Letter 27, 024703.
31. Naveed M, Abbas Z, Sajid M (2015) Hydromagnetic flow over an unsteady curved stretching surface. Eng Sci Tech, Int J doi: 10.1016/j.jestch.2015.11.009
32. Rosca NC, Pop I (2015) Unsteady boundary layer flow over a permeable curved stretching/shrinking surface. Europ J Mech B/Fluids 51, 61–67.
33. Abbas Z, Naveed M, Sajid M (2016) Hydromagnetic slip flow of nanofluid over a curved stretching surface with heat generation and thermal radiation. J Mol Liq 215, 756–762.
34. Ganji DD, Abbasi M, Rahimi J, Gholami M,Rahimipetroudi I (2014) On the MHD squeeze flow between two parallel disks with suction or injection via HAM and HPM. Front Mech Eng 9, 270–280.
35. Abbasbandy S, Yurusoy M, Gulluce H (2014) Analytical solutions of non-linear equations of power-law fluids of second grade over an infinite porous plate. Math Compu Appl 19, 124.
36. Sui J, Zheng L, Zhang X, Chen G (2015) Mixed convection heat transfer in power law fluids over a moving conveyor along an inclined plate. Int J Heat Mass Transf 85, 1023–1033.
37. Farooq U, Hayat T, Alsaedi A, Liao SJ (2015) Series solutions of non-similarity boundary layer flows of nano-fluids over stretching surface. Numer Algor 70, 43–59.
38. Hayat T, Qayyum S, Imtiaz M, Alzahrani F, Alsaedi A (2016) Partial slip effect in flow of magnetite-Fe_3O_4 nanoparticles between rotating stretchable disks. J Magn Magn Mater 413, 39–48.
39. Mustafa M (2015) Cattaneo-Christov heat flux model for rotating flow and heat transfer of upper-convected Maxwell fluid. AIP Adv 5, 047109.

40. Hayat T, Imtiaz M, Alsaedi A,Alzahrani F (2016) Effects of homogeneous—heterogeneous reactions in flow of magnetite-Fe_3O_4 nanoparticles by a rotating disk. J Mol Liq 216, 845–855.

41. Hatami M, Nouri R, Ganji DD (2013) Forced convection analysis for MHD Al_2O_3-water nanofluid flow over a horizontal plate. J Mol Liq 187, 294–301.

42. Ellahi R, Hassan M, Zeeshan A (2015) Shape effects of nanosize particles in Cu-H_2O nanofluid on entropy generation. Int J Heat Mass Transf 81, 449–456.

43. Hayat T, Hussain Q, Javed T (2009) The modified decomposition method and Pade approximants for the MHD flow over a nonlinear stretching sheet. Nonlinear Anal: Real World Appl 10, 966–973.

44. Mabood F, Das K (2016) Melting heat transfer on hydromagnetic flow of a nanofluid over a stretching sheet with radiation and second-order slip. Europ Phy J Plus 131, 3.